

Co-Designing Robots by Differentiating Motion Solvers

Traiko Dinev, Carlos Mastalli, Vladimir Ivan, Steve Tonneau, Sethu Vijayakumar

Abstract—We present a novel algorithm for the computational co-design of legged robots and dynamic maneuvers. Current state-of-the-art approaches are based on random sampling or concurrent optimization. A few recently proposed methods explore the relationship between the gradient of the optimal motion and robot design. Inspired by these approaches, we propose a bilevel optimization approach that exploits the derivatives of the motion planning sub-problem (the inner level) without simplifying assumptions on its structure. Our approach can quickly optimize the robot’s morphology while considering its full dynamics, joint limits and physical constraints such as friction cones. It has a faster convergence rate and greater scalability for larger design problems than state-of-the-art approaches based on sampling methods. It also allows us to handle constraints such as the actuation limits, which are important for co-designing dynamic maneuvers. We demonstrate these capabilities by studying jumping and trotting gaits under different design metrics and verify our results in a physics simulator. For these cases, our algorithm converges in less than a third of the number of iterations needed for sampling approaches, and the computation time scales linearly.

I. INTRODUCTION

A traditional approach to robot design consists of iterations between mechanical design and motion planning (e.g., [1]). With the increase in complexity of modern robots, this becomes a challenging task as designers need to consider both the efficiency of the robot as well as the ability to execute the desired motions. Thus, *expert specialists* designers and many design iterations are needed.

Concurrent design (co-design [2]) aims to automate this process by optimizing both the motions and design parameters together. In the context of quadrupeds, motions are specified as high-level tasks, such as a jump or a forward trot and solved by a motion planner. The design parameters can for instance consist of the morphology of the robot – the lengths of its limbs and body. By using a metric of efficiency, such as the mechanical cost of transport, the co-design algorithm can optimize the robot’s design parameters for it to more efficiently execute the specified task.

A. Related Work

We classify current co-design approaches into two broad categories: *sampling-based* and *gradient-based* methods.

All authors are with the Edinburgh Centre for Robotics, University of Edinburgh, UK.

This research was supported by (1) the European Commission under the Horizon 2020 project Memory of Motion (MEMMO, ID: 780684) and (2) the Engineering and Physical Sciences Research Council (EPSRC), and (3) the Alan Turing Institute.

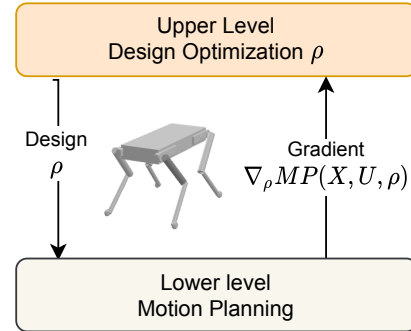


Fig. 1: Illustration of our bilevel optimization approach for robot co-design. In the upper level we use gradient information from the motion planning (lower level) to optimize the design of the robot in an iterative fashion. Please find the accompanying video at <https://youtu.be/YQ22T5sBbxA>

1) *Sampling-based methods*: These methods exploit variants of Monte-Carlo sampling to find candidate robot designs. The fitness of those candidates is evaluated in a second stage through a motion planning program. These methods are thus formulated as a two-stage problem.

The Covariance Matrix Adaptation Evolutionary Strategy (CMA-ES) [3] is a popular sampling approach used in co-design. It uses a Gaussian prior on candidate design parameters and estimates a covariance matrix needed for the following sampling steps. Its main advantages are that i) with a large enough covariance, it can escape local minima by sampling a wider range of designs and ii) it can use any motion planner in the inner loop regardless of its differentiability property. However, in practice, CMA-ES does not scale well with respect to the number of design parameters (i.e., decision variables) due to the curse of dimensionality.

Despite this limitation, evolutionary strategies have attracted major research attention due to the above-mentioned flexibility of the motion optimization. For instance, Wampler et al. [3] used a variant of CMA-ES to co-design various creatures in simulation, and Digumarti et al. [4] co-designed the legs of the quadruped StarLETH to optimize its running speed. Most recently, Chadwick et al. [5] optimized the legs of quadrupeds and bipeds over uneven terrain for different user-defined co-design metrics, and Fadini et al. [6] computed the actuator properties of a monopod using CMA-ES.

2) *Gradient-based methods*: An alternative approach is to directly consider the effects of optimal motions on the design parameters by optimizing them together. The major drawback of this approach is the complexity of the resulting

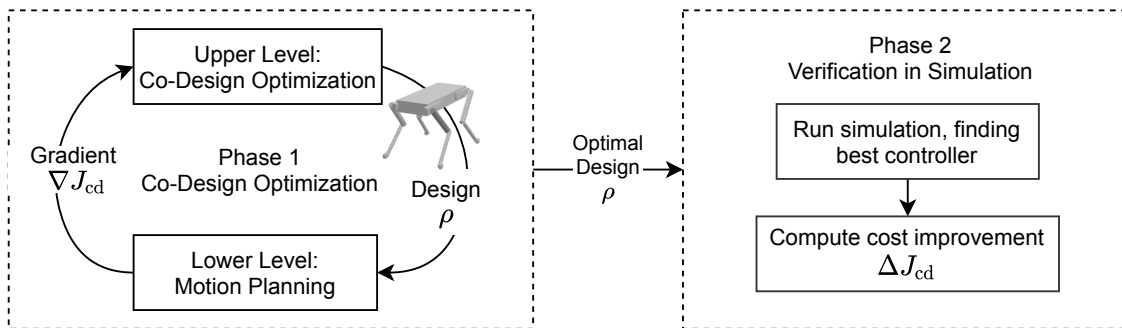


Fig. 2: A schematic of our co-design pipeline. In the first phase we optimize the robot’s design by differentiating through a motion planner (a nonlinear optimal control problem). Then, we verify the design improvements in a physics simulator using a proportional-derivative (PD) controller to track the motion plan.

nonlinear program. Nonetheless, this approach has also attracted attention for the co-design of legged robots. For instance, Mombaur [7], Buondonno et al. [8] and Spielberg et al. [9] embedded design and motion optimizations in a single nonlinear program to compute the lengths of the robot limbs and/or actuator parameters. These methods use different dynamics models: rigid-contact dynamics [7], full dynamics with elastic actuators [8] and contact-implicit dynamics [9].

A few recent pieces of work have contributed to a new way of treating the co-design optimization problem. Ha et al. [10] proposed to extract the relationship between motion and design by using the implicit function theorem. This allowed them to optimize the design while keeping the motion on the manifold of optimal motions. In a similar fashion, Desai et al. [11] used sensitivity analysis and the adjoint method to determine the same relationship. This latter approach was used in [12] and [13] for human-in-the-loop design optimization of robots.

The approach of [10] relies on user input to specify which design parameters in the optimization to change. In contrast, the approach used in [11]–[13] allows for optimization of all design parameters given high-level task descriptions. One significant drawback of [11]–[13] is that the motion is computed as an unconstrained minimization, which makes it more difficult to design the motion task but it helps to easily derive the relationship between motion and design.

In this paper we demonstrate a more general solution, where we directly take the derivative of the motion planner without considering the underlying optimization explicitly by treating it as a generic nonlinear function. Our approach contains an upper and a lower-level optimization for robot design and motion planning, respectively. It also allows us to use efficient constrained motion planners and to modify the design optimization without modifying the motion plan. In fact we can use any continuously differentiable motion planner. Additionally, user inputs are not required, other than to specify the co-design metric and motion task. Below we describe the technical contributions of our work.

B. Contributions

The main contribution of our work is a novel bilevel optimization approach for robot co-design (see Fig. 1). Here

we identify four technical contributions:

- i. a computational co-design algorithm that explicitly differentiates a motion planner;
- ii. a co-design pipeline that incorporates a verification step in simulation;
- iii. comparisons against a sampling method based on CMA-ES: fast convergence rate, greater scalability and computational speed; and
- iv. an experimental demonstration of the effects of using a constrained motion planner.

Our approach goes beyond state-of-the-art approaches as it uses first principles of bilevel optimization, numerical optimal control and sensitivity analysis for handling the full dynamics of the system, joint limits, and the co-design parameter bounds. In order to do so, we formulate a bilevel optimization problem where we optimize the motion in the lower level, compute the gradient of the motion planner and use it to optimize the design in the upper level.

II. CO-DESIGN PIPELINE

Our co-design pipeline has two phases as shown in Fig. 2. In the first phase, we optimize the design and the motion of a robot using a gradient approach. In the second phase, we verify our results in a physics simulator. Below we describe each of the three main components of our framework: co-design optimization, motion planning, and verification in simulation.

A. Co-design as bilevel optimization

We begin by encoding the robot’s design into a *design vector* ρ . In this paper, ρ encodes the robot’s link lengths and its base shape (width, height, depth). We then formulate the co-design problem over the design vector ρ as a bilevel optimization problem:

$$\begin{aligned}
 \min_{\rho, \mathbf{X}, \mathbf{U}} \quad & J_{cd}(\rho, \mathbf{X}, \mathbf{U}) && \text{(co-design metric)} \\
 \text{s.t.} \quad & \mathbf{X}, \mathbf{U} = \text{MP}(\rho; \text{TASK}), && \text{(motion planning)} \\
 & \underline{\rho} \leq \rho \leq \bar{\rho}, && \text{(design bounds)}
 \end{aligned} \tag{1}$$

Algorithm 1 Co-design optimization

- 1: Start at a design $\rho = \rho_0$
 - 2: **while** $J_{\text{cd}}(\rho, \mathbf{X}, \mathbf{U})$ decreasing or at max. iteration **do**
 - 3: Compute $\nabla_{\rho} J_{\text{cd}}$ in parallel, using warmstart \mathbf{U}_{ws}
 - 4: Save the resulting trajectory to \mathbf{U}_{ws} and cost J_{cd}
 - 5: Update $\rho \leftarrow \rho - \eta \nabla_{\rho} J_{\text{cd}}$
 - 6: **end while**
 - 7: **return** (ρ, J_{cd}) – optimal design and its cost value
-

where $J_{\text{cd}}(\cdot)$ is a user-specified co-design metric that evaluates the goodness of a design, $\text{MP}(\cdot)$ is the motion planning function, $\underline{\rho}$ and $\bar{\rho}$ are the lower and upper bounds of the design parameters. The co-design metric J_{cd} evaluates the efficiency of locomotion (e.g., mechanical cost of transport) and high-level robot design specifications (e.g, symmetrical legs). The MP function describes a nonlinear optimal control problem, which computes a discretized trajectory of robot states – $\mathbf{X} = \{\mathbf{x}_0, \dots, \mathbf{x}_N\}$ and controls $\mathbf{U} = \{\mathbf{u}_0, \dots, \mathbf{u}_{N-1}\}$ – for a desired task (represented by TASK) such as a trotting or jumping gait. Here N is the planning horizon, which is part of the task description.

Our approach sequentially optimizes both the design vector ρ and the whole-body motion $\mathbf{m} = \{\mathbf{X}, \mathbf{U}\}$ for a given task. In the upper level we optimize the motion by using gradients from the motion planning lower level. We formulate the lower level (the motion planner MP) as a hybrid nonlinear optimal control problem. MP thus generates an optimal motion while considering the robot’s full dynamics, its joint limits and contact interactions as described in Section II-B.

The motion planner itself can be treated as a function that computes an optimal trajectory $\{\mathbf{X}, \mathbf{U}\}$ for a given design vector ρ under a pre-specified task. Therefore, we can compute the derivative of the co-design cost J_{cd} with respect to ρ as

$$\begin{aligned} \nabla_{\rho} J_{\text{cd}} &= \frac{dJ_{\text{cd}}(\rho, \mathbf{m})}{d\rho} = \frac{\partial J_{\text{cd}}}{\partial \mathbf{m}} \frac{\partial \mathbf{m}}{\partial \rho} + \frac{\partial J_{\text{cd}}}{\partial \rho}, \\ &= \frac{\partial J_{\text{cd}}}{\partial \mathbf{m}} \frac{\partial \text{MP}(\rho; \text{TASK})}{\partial \rho} + \frac{\partial J_{\text{cd}}}{\partial \rho}, \end{aligned} \quad (2)$$

where $\frac{\partial \mathbf{m}}{\partial \rho}$ is the derivative of the motion with respect to the design parameters. Amos et al. [14] demonstrated that indeed nonlinear programs, such as our motion planner, are differentiable. Here we obtain $\nabla_{\rho} J_{\text{cd}}$ through a numerical differentiation procedure that runs in parallel, i.e., we compute the derivative for each component of the design vector using multiprocessing.

Using the derivative $\nabla_{\rho} J_{\text{cd}}$, we can then optimize the design based on a variant of the gradient descent algorithm:

$$\rho_{i+1} = \rho_i - \eta \frac{dJ_{\text{cd}}(\rho, \mathbf{m})}{d\rho},$$

where $\eta \in \mathbb{R}_+$ is the *learning rate*. We used ADAM [15], as it has good convergence properties and automatically scales the learning rate η (a common limitation of the steepest descent direction). Lastly, we warm-start the inner optimization iterations from the previous best control trajectory \mathbf{U}_{ws}

to speed up convergence. We present the entire co-design optimization algorithm in Algorithm 1.

The key difference between [12], [11], and our method is in the computation of $\frac{\partial \mathbf{m}}{\partial \rho}$. The authors in [11] used the adjoint method to compute this derivative. The authors in [12] do not address the computation explicitly, however both use the same update rule. For comparison, we describe the update rule and its derivation in detail in the Appendix. We also note that this update rule from [12] is only valid for unconstrained motion planning as described in the Appendix.

In contrast, our approach directly considers the motion as a function of the motion planner and does not assume a particular form of motion planning. We then take the derivative of the entire algorithm. We use finite differences to compute the derivative $\nabla_{\rho} J_{\text{cd}}$ directly, which has linear complexity in the dimension of ρ .

Our method allows us to use the full rigid body dynamics, friction cone constraints, control and state bounds in a nonlinear optimal control formulation (motion planner). To illustrate the benefits of our co-design approach, we provide experimental results that specifically consider torque limits for robot co-design in Section IV-B.

B. Motion planning

The lower level of our co-design bilevel optimization algorithm computes the motion trajectory $\{\mathbf{X}, \mathbf{U}\}$ given a task and design ρ . We formulate this inner optimization as a hybrid nonlinear optimal control problem with fixed contact sequence and timings:

$$\begin{aligned} \arg \min_{\mathbf{X}, \mathbf{U}} \quad & \sum_{k=0}^{N-1} \|\mathbf{q}_k \ominus \mathbf{q}_{\text{ref}}\|_{\mathcal{Q}}^2 + \|\mathbf{v}_k\|_N^2 + \|\mathbf{u}_k\|_R^2 + \|\boldsymbol{\lambda}_k\|_{\mathcal{K}} \\ \text{s.t.} \quad & \\ & \text{for each contact phase: } p \in \mathcal{P} = \{1, 2, \dots, N_p\} \\ & \text{if } \underline{\Delta}t_p \leq k \leq \bar{\Delta}t_p: \\ & \quad \mathbf{q}_{k+1} = \mathbf{q}_k \oplus \int_{t_k}^{t_k + \Delta t_k} \mathbf{v}_k dt, \quad (\text{integrator}) \\ & \quad \mathbf{v}_{k+1} = \mathbf{v}_k + \int_{t_k}^{t_k + \Delta t_k} \dot{\mathbf{v}}_k dt, \\ & \quad (\dot{\mathbf{v}}_k, \boldsymbol{\lambda}_k) = \mathbf{f}_p(\mathbf{q}_k, \mathbf{v}_k, \mathbf{u}_k), \quad (\text{contact dyn.}) \\ & \text{else:} \\ & \quad \mathbf{q}_{k+1} = \mathbf{q}_k, \\ & \quad (\mathbf{v}_{k+1}, \boldsymbol{\lambda}_k) = \mathbf{\Delta}_p(\mathbf{q}_k, \mathbf{v}_k), \quad (\text{impulse dyn.}) \\ & \quad \mathbf{g}(\mathbf{q}_k, \mathbf{v}_k, \mathbf{u}_k) = \mathbf{0}, \quad (\text{equality}) \\ & \quad \mathbf{h}(\mathbf{q}_k, \mathbf{v}_k, \mathbf{u}_k) \leq \mathbf{0}, \quad (\text{inequality}) \\ & \quad \underline{\mathbf{x}} \leq \mathbf{x}_k \leq \bar{\mathbf{x}}, \quad (\text{state bounds}) \\ & \quad \underline{\mathbf{u}} \leq \mathbf{u}_k \leq \bar{\mathbf{u}}. \quad (\text{control bounds}) \end{aligned} \quad (3)$$

The state $(\mathbf{q}, \mathbf{v}) \in X$ lies in a differential manifold formed by the configuration $\mathbf{q} \in \mathbb{SE}(3) \times \mathbb{R}^{n_j}$ and its tangent vector $\mathbf{v} \in \mathbb{R}^{n_x}$ (with n_x and n_j as the dimension of the state manifold and number of joints, respectively). The control $\mathbf{u} \in \mathbb{R}^{n_j}$ is the vector of input torques, \ominus and \oplus are the

difference and *integration* operators of the state manifold, respectively. Then \mathbf{q}_{ref} is the reference robot posture, and $\mathbf{f}_p(\cdot)$ represents the contact dynamics under the phase p . To account for effects of discrete contact changes, $\Delta_p(\cdot)$ is used to define an autonomous system that describes the contact-gain transition.¹ \mathbf{Q} , \mathbf{N} , \mathbf{R} and \mathbf{K} are positive-definite weighting matrices, $(\underline{\mathbf{x}}, \bar{\mathbf{x}})$ and $(\underline{\mathbf{u}}, \bar{\mathbf{u}})$ are the lower and upper bounds of the system state and control. $\underline{\Delta}t_p$ and $\bar{\Delta}t_p$ defines the timings of the contact phase p . Below we provide more details about the hybrid dynamics, constraints and problem resolution. The hybrid dynamics implicitly compute the contact forces λ_k by assuming a rigid interaction (e.g., as in [17]).

1) *Hybrid dynamics*: The hybrid system is composed of contact and impulse dynamics, i.e.,

$$\begin{bmatrix} \dot{\mathbf{v}} \\ -\lambda \end{bmatrix} = \begin{bmatrix} \mathbf{M} & \mathbf{J}_c^\top \\ \mathbf{J}_c & \mathbf{0} \end{bmatrix}^{-1} \begin{bmatrix} \boldsymbol{\tau}_b \\ -\mathbf{a}_0 \end{bmatrix} \text{ or} \\ \begin{bmatrix} \mathbf{v}^+ \\ -\lambda \end{bmatrix} = \begin{bmatrix} \mathbf{M} & \mathbf{J}_c^\top \\ \mathbf{J}_c & \mathbf{0} \end{bmatrix}^{-1} \begin{bmatrix} \mathbf{M}\mathbf{v}^- \\ -e\mathbf{J}_c\dot{\mathbf{v}}^- \end{bmatrix},$$

respectively. Both dynamics describe a rigid contact where \mathbf{M} is the joint-space inertia matrix and \mathbf{J}_c is the contact Jacobian expressed in the local frame. $\boldsymbol{\tau}_b = \mathbf{S}\mathbf{u} - \mathbf{b}$ is the force-bias vector that accounts for the selected torque commands, Coriolis and gravitational effects. \mathbf{a}_0 is the desired acceleration in the constraint space (with Baumgarte stabilization as described in [18]). $e \in [0, 1]$ is the restitution coefficient, \mathbf{v}^- and \mathbf{v}^+ are generalized velocities before and after the impulse, respectively. We compute the hybrid dynamics and its derivatives as described in [18].

2) *Constraints*: Both inequality and equality constraints are defined for swing and contact phases. During contact phases, we only include friction-cone constraint via a linearized cone:

$$\mathbf{A}\lambda_{\mathcal{C}(k)} \leq \mathbf{r},$$

where (\mathbf{A}, \mathbf{r}) are computed from a predefined number of edges, and minimum and maximum normal contact forces, respectively. $\mathcal{C}(k)$ describes the set of active contacts. In contrast, during the swing phases, we include contact-placement constraints:

$$\log(\mathbf{p}_{\mathcal{G}(k)}^{-1} \circ \mathbf{M}_{\mathbf{p}_{\mathcal{G}(k)}}) = \mathbf{0},$$

where $\log(\cdot)$ describes the log operator used in Lie algebra, $\mathbf{p}_{\mathcal{G}(k)}$ and $\mathbf{M}_{\mathbf{p}_{\mathcal{G}(k)}}$ are the reference and current placements of the set of swing contacts $\mathcal{G}(k)$.

3) *Optimal control resolution*: We solve the motion planning problem formulated in Eq. (3) with Feasibility-Driven Control-limited DDP (BOX-FDDP) [19], which is a variant of the Differential Dynamic Programming (DDP) algorithm. BOX-FDDP uses direct-indirect hybridization and enforces hard-constraints for the control limits. We employ a soft quadratic barrier to enforce inequality, equality and state constraints defined in Eq. (3). We implemented the algorithm using the open-source library CROCODDYL [18].

¹The term *contact-gain* was introduced in [16].

C. Verification in simulation

The second phase of our co-design pipeline validates the design improvements in the PYBULLET physics simulator. To do so, we execute the motion plan for both the nominal and the optimized designs, and record the costs J_{cd} . Then, we compare the costs between optimization and simulation results, and record a percentage improvement ΔJ_{cd} (similar to [20]). With this metric, we account for the difference in time discretization as the integrator in Eq. (3) can be seen as a proxy function.

We use a proportional-derivative (PD) controller with feed-forward torque to track the planned motion:

$$\mathbf{u} = \mathbf{u}^* + \mathbf{K}_p(\mathbf{q}_j^* - \mathbf{q}_j) + \mathbf{K}_d(\mathbf{v}_j^* - \mathbf{v}_j),$$

where \mathbf{u}^* , \mathbf{q}_j^* and \mathbf{v}^* are the reference feed-forward command, joint positions and velocities computed in Eq. (3), respectively. \mathbf{K}_p and \mathbf{K}_d are the PD gains. We tune these gains through a grid search procedure. We run the simulator on a 10×10 grid for $\mathbf{K}_p \in [1, 20]$ and $\mathbf{K}_d \in [0.1, \mathbf{K}_d/2]$. Then, we pick the gains that lead to the smallest tracking error for both designs. Note that this procedure allows us to fairly compare and account for different robot dimensions and weights, as larger robots require higher gains and vice-versa. Below, we provide more details about the co-design parameters and cost metrics used in this work.

III. CO-DESIGN PARAMETERS

We focus our work on improving the design of the 12 Degrees of Freedom (DoFs) SOLO robot [21]. Particularly, we are interested in quadrupedal locomotion gaits such as trotting and jumping. Here, we provide details of the used design vector and cost metrics.

A. Co-design on the Solo robot

Our design vector $\boldsymbol{\rho}$ consists of the lengths of the lower- and upper-leg limbs, and the trunk shape: width, height and depth. To formulate a proper co-design problem for the SOLO robot, we make the following assumptions. First, for the lower-leg limbs, we consider that the masses are proportional to their lengths as they are entirely 3D-printed and the motors are attached to the hip joints (i.e., they do not contribute to the mass of the lower limbs).² Instead, for the upper-leg limbs, we consider that only 95g (36%) of their total masses are proportional to the link lengths and the outstanding masses are contributed by the motors, motor shafts and pulleys. Second, we consider that the body mass is independent of its volume, and it is represented by a 1kg box centered in the middle of the body. The total mass of the nominal SOLO trunk is 1.16kg. In our simplified model, we ignore the 3D-printed component, as the trunk weight is dominated by the on-board electronics and sensors. Furthermore, we implicitly constrain (by clipping) the upper limb lengths to be less than half the width of the robot. With this, we prevent self-collision as this design simplifies planning and control algorithms. Finally,

²We note that this is true for the foot with no contact switch.

we define the box constraints for each of the parameters in ρ as

$$\begin{aligned} 0.125\text{m} &\leq l_{\text{lower}} \leq 0.4\text{m}, \\ 0.125\text{m} &\leq l_{\text{upper}} \leq 0.4\text{m}, \\ 0.375\text{m} &\leq w_{\text{trunk}} \leq 1.0\text{m}, \\ 0.15\text{m} &\leq h_{\text{trunk}} \leq 1.0\text{m}, \\ 0.05\text{m} &\leq d_{\text{trunk}} \leq 0.2\text{m}, \end{aligned}$$

where l_{lower} and l_{upper} are the lengths of the lower- and upper-leg limbs. w_{trunk} , h_{trunk} and d_{trunk} are the width, height and depth of the robot trunk, respectively. Note that the bounds for the lower- and upper-leg limbs are the same. However, we use different bounds for the trunk to avoid self-collision and collision with the ground.

B. Co-design costs

Next, we specify the three different co-design costs we used and their physical meanings. The first cost is the Cumulative square Joint Torque (CJT):

$$J_{\text{CJT}} = \sum_{k=0}^{N-1} \|\mathbf{u}_k\|^2.$$

This cost is differentiable and often used in motion control to penalize large torques (e.g., [22]). Additionally, it can be used as a simple proxy to encourage more energy-efficient motion.

The second cost is the Mechanical Cost of Transport (MCOT). The MCOT is often used to measure the locomotion efficiency of legged robots (e.g., [23]), which is inspired by the metabolic cost of transport used to analyze their biological counterpart. Concretely, we compute as the average velocity divided by the average power (as described in [5]):

$$J_{\text{MCOT}} = \sum_{\text{leg } l} \frac{P_l}{m_l g (v_x + v_y)},$$

where m_l is the mass supported by the leg (1/4 of the trunk mass together with the leg mass), g is gravity. P_l , v_{x_k} and v_{y_k} are the absolute mean power per leg and trunk velocities in the x and y direction at time k , respectively. Note that we do not consider the z-velocity for either gaits. For trotting there is no motion in the z-direction (i.e., locomotion on flat terrain) and for jumping the z-motion sums to zero since the robot follows a ballistic trajectory.

Lastly, we consider the Peak Torque (PT) of the actuators as a co-design metric, i.e.,

$$J_{\text{PT}} = \max_{k,j} u_{j_k},$$

where u_{j_k} is torque command of joint j at time k . One important remark is that J_{PT} is neither convex nor differentiable as it uses a max-operator. Therefore, optimizing over it via gradient descent is not recommended. Nonetheless, it is of research interest to study the practical effects of using it for co-design, specifically in the comparisons against state-of-the-art genetic algorithms (CMA-ES [24]). Note that the CMA-ES algorithms can optimize over any well-defined cost without imposing a differentiability or smoothness condition.

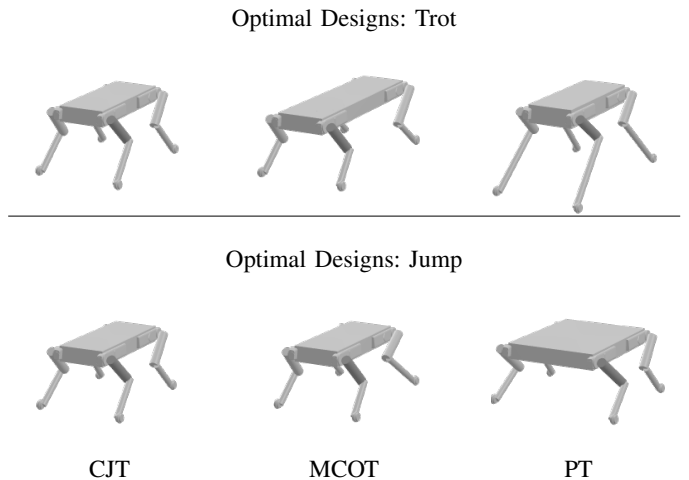


Fig. 3: Optimal designs for the jumping and trotting tasks obtained using the three different co-design metrics. Smaller robots are preferred for jumping than for trotting gaits, as the former task requires higher torque commands and swing motions.

C. Symmetry cost

Finally, for all robots and tasks we add a quadratic symmetry penalty between the pairs of front and back legs:

$$J_{\text{sym}} = \sum_{p = \text{low, up}} (l_p^{\text{front}} - l_p^{\text{back}})^2 + (l_p^{\text{hind}} - l_p^{\text{fore}})^2,$$

where l_p^{front} , l_p^{hind} are the lengths of the p limb (lower or upper) for the front and hind legs, respectively.

IV. EXPERIMENTS

In our experiments, we considered two tasks – trotting and jumping forward. For both tasks, we ran our pipeline (Fig. 2) for all three co-design metrics. We carried out all experiments on a desktop machine using an Intel(R) Core(TM) i9-9900K CPU at 3.6 GHz and 64 GB 3000 MHz memory.

A. Co-design results under different metrics

In this section, we report the results of our co-design pipeline: co-design optimization and simulation verification. We studied a forward trotting and a jumping task under the above-mentioned metrics.

1) *Trotting*: In this experiment, we optimized both the robot design and motions for a forward trotting task. The high-level motion task is to take two steps forward, each of 0.05m, with a fixed step height of 0.05m. We allocated 25 and 15 knots for the swing and double support phases of the motion, respectively, and used a symplectic Euler integrator with time-step of 10ms. We ran our co-design algorithm with the three co-design metrics described above, namely J_{CJT} , J_{MCOT} and J_{PT} . We show the resulting designs in Fig. 3. We report the resulting cost percentage improvement between initial and final costs ΔJ_{cd} for both the first and the second phase in Table I.

A common feature between all designs is the smaller upper legs. The designs for J_{CJT} and J_{PT} are similar with a taller

		ΔJ_{CJT}	ΔJ_{MCOT}	ΔJ_{PT}
trot	opt	-61.53%	-53.39%	-56.71%
	sim	-62.43%	-60.28%	-53.15%
jump	opt	-61.11%	-46.23%	-42.17%
	sim	-62.37%	-60.44%	-41.03%

TABLE I: Cost improvement percentage in optimization and simulation for all co-design metrics and two tasks.

and shorter body, whereas for J_{MCOT} the body is longer and the top legs are at the minimum of the design bounds. For all three co-design metrics, the cost improvements ΔJ_{cd} remained within 10% in simulation with J_{MCOT} having the largest margin and J_{CJT} showing a 6.89% more improvement in simulation.

2) *Jumping*: Here we considered optimizing the design and motion for a jumping task. The high-level motion task is to jump forward 0.1m with a step height of 0.15m. We used the same integrator and time-step as in the trotting case. We defined 15 knots for the flight phase and 25 knots for the take-off and landing phases. For all the co-design metrics, we report the resulting designs in Fig. 3 and the cost improvements in Table I.

In general, our co-design algorithm selected a smaller robot for jumping than for trotting tasks under J_{CJT} and J_{MCOT} . However, these results validate what is intuitively expected for metrics that aim to minimize motion energy. Furthermore, J_{CJT} and J_{PT} differ in the shape of the trunk, with a wider trunk found when optimizing peak torque, as the latter metric does not penalize energy. As in the trotting case, the cost improvement difference between simulation and optimization are within 10% for J_{CJT} and J_{PT} . Instead, for J_{MCOT} , we see a 14.21% improvement in simulation.

B. Design optimization with restrictive actuation limits

Next, we studied the effects of using weak actuators in the knees when carrying a payload. We reduced the knee torque limits to $\pm 5.0 \text{ N} \cdot \text{m}$ while also adding a 0.5kg payload on the back of the robot, represented as the yellow box in Fig. 4. The high-level task was to jump 0.075m with 0.1m of step height. We used the J_{MCOT} metric for optimizing the design. Note that we reduced the jumping length and height due to the increased mass of the robot.

The resulting designs and their knee torque commands are shown in Fig. 4 and Fig. 5, respectively. With the restrictive joint limits our algorithm finds a smaller robot in terms of both trunk and hind leg widths. It leads to smaller output torques for the optimized designs in the resulting motion plan. These results show that co-designing with constraints such as joint limits might lead to different optimal designs. This, however, comes at an increased computational time—from 16 to 31 seconds—as the co-design algorithm often needs to perform more iterations for satisfying the torque constraints. Nonetheless, both the computational times are under a minute, as the problem complexity remains the same

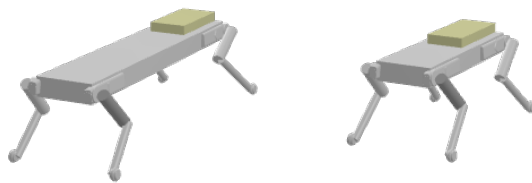


Fig. 4: Co-optimizing a jumping with payload for the SOLO torque limits (left) and for restrictive torque limits in the knee joints (right). As expected, our algorithm designed a smaller robot, in both the trunk width and the hind leg length, to achieve a jumping task with the limited actuator capabilities.

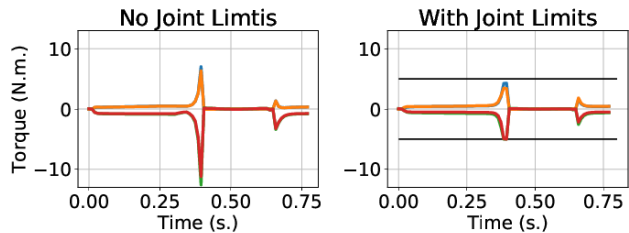


Fig. 5: Knee torque commands without restrictive joint limits (left) and with (right) for the payload jumping task.

(i.e., same dimension for the system dynamics, planning horizon and co-design vector).

A fast computational time is indeed a key feature of a co-design algorithm, as it can enable fast evaluation of different designs and metrics. Next, we compare the convergence and scalability properties of our algorithm against the genetic algorithm CMA-ES.

C. Comparison with a genetic algorithm

We compared our gradient-based co-design approach to the CMA-ES genetic algorithm on the trotting task for all the three co-design metrics. We used the open-source CMA-ES library PYCMA library [25].

1) *Convergence and computation time*: To make a fair comparison, we vary CMA-ES' hyper-parameters as it is a stochastic algorithm. The two hyper-parameters of interests are the population size N_{pop} and its initial standard deviation σ , as they define how many candidate designs are sample in each iteration and how far away from the starting design the algorithm samples, respectively. Indeed, both hyper-parameters can be used to define the balance between exploration and exploitation and thus have a significant effect on convergence.

Concretely, we used a 3×3 grid to change both hyper-parameters as

$$N_{pop} \in [10, 20, 50],$$

$$\sigma \in \left[\frac{b}{2}, \frac{b}{3}, \frac{b}{4} \right],$$

where we scaled $\rho \in [-b, b]$, with $b = 10$, which was needed to enforce the design bounds as described in Eq. (1). This was

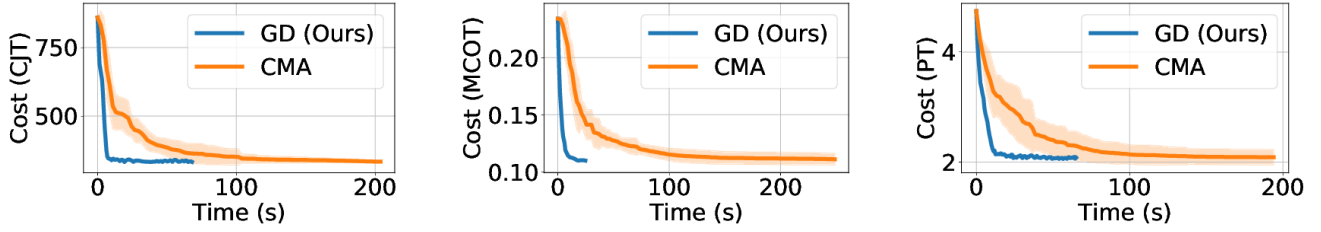


Fig. 6: Convergence comparison of GD-based co-design and CMA-ES over the trotting task over both time and iteration. GD stands for gradient descent.

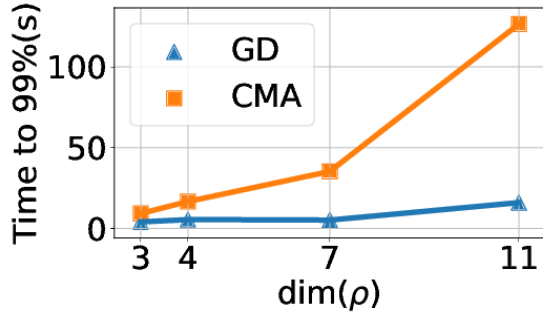


Fig. 7: Scalability to different ρ dimensions for the trotting task with the cumulative joint torque metric.

needed since CMA-ES does not handle constraints directly, and it is in fact the recommended approach in PyCMA [25].

We plot the mean cost and standard deviation in Fig. 6. To do so, we recorded the best design ρ obtained overall to compute the intermediate costs. Additionally, we report the computation time (mean and standard variation) in Fig. 6. Although performance *per iteration* between CMA-ES and our approach is similar, our method has a faster convergence in time as it exploits the derivative of the motion planner. However, this is at the risk of getting stuck in local minima. For instance, we can see this effect for the MCOT metric, where CMA-ES computes a design with lower cost. On the other hand, we observed that gradient descent having poorer convergence with sudden jumps for the PT metric, which it is expected for a non-smooth function. Nevertheless, this result shows that, in practice, our approach can still optimize a non-differentiable co-design cost. Next we examine the scalability of our approach and CMA-ES.

2) *Scalability study:* We studied how the convergence time scales with the design vector ρ size for both CMA-ES and our approach. For this comparison, we used the CJT metric and a trotting gait. We report the computation time for the following design vector sizes:

- 1) $\dim(\rho) = 3$ for trunk shape (width / height / depth)
- 2) $\dim(\rho) = 4$ for upper-leg limbs
- 3) $\dim(\rho) = 7$ for upper-leg limbs and trunk shape
- 4) $\dim(\rho) = 11$ for trunk shape, and upper- and lower-leg limbs

For each case we ran CMA-ES only once with $N_{\text{pop}} = 20$ and $\sigma = 5.0$ since we observed a relatively small standard deviation in the cost values reported in the previous experiment. Note that this is also the recommended standard deviation given the scaling bounds [25]. We report the convergence time at 99% cost improvement in Fig. 7, as we observed a long trail that never triggered the termination criterion in the CMA-ES case (see Fig. 6).

Our approach scales better as the dimension of ρ increases. For lower-dimensional problems, the difference in time and number of iterations are smaller, as the solution is easily found by both sampling and gradient descent approaches. However, sampling approaches have a slower convergence time for more complex co-design problems. Indeed, they are often used for problems of moderate dimensions as for instance reported in [24].

V. DISCUSSION AND FUTURE WORK

In this paper we proposed a novel co-design algorithm and pipeline for dynamic quadruped locomotion. Our approach is based on bilevel optimization and exploits the derivatives of a hybrid nonlinear optimal control problem (inner problem that describes the motion planner).

When compared to state-of-the-art approaches based on CMA-ES, our method finds locally optimal solutions faster. However, depending on the co-design metric, CMA-ES can find a more optimal solution (that is, a solution with a lower cost). Nevertheless, our approach has better scalability than CMA-ES, which potentially allows us to resolve more complex co-design problems in a shorter amount of time.

Currently, our approach only handles continuous design parameters. However, it could be extended in such a way that can handle discrete variables in the future. Moreover, we reported results using finite differences, which is not as efficient as analytical derivatives, which only add a small computational burden to the optimal control problem [14]. Therefore we expect a significant reduction in computation time for larger design vectors when using analytical derivatives. On the other hand, our bilevel optimization approach can be scaled to more complex design vectors, for instance by including gear ratios, equipment locations (e.g., battery and PCs) or actuator parameters (e.g., stiffness constant in serial elastic actuators). Due to its computational efficiency,

it can also be used for computer-aided design in a fashion similar to [12] and [13].

REFERENCES

- [1] C. Semini, N. G. Tsagarakis, E. Guglielmino, M. Focchi, F. Cannella, and D. G. Caldwell, "Design of HyQ - a hydraulically and electrically actuated quadruped robot," *Journal of Systems and Control Engineering*, vol. 225, 2011.
- [2] Q. Li, W. Zhang, and L. Chen, "Design for control-a concurrent engineering approach for mechatronic systems design," vol. 6, 2001.
- [3] K. Wampler and Z. Popović, "Optimal gait and form for animal locomotion," *ACM Transactions on Graphics*, vol. 28, 2009.
- [4] K. M. Digumarti, C. Gehring, S. Coros, J. Hwangbo, and R. Siegwart, "Concurrent optimization of mechanical design and locomotion control of a legged robot," in *Mobile Service Robotics*. World Scientific, 2014.
- [5] M. Chadwick, H. Kolvenbach, F. Dubois, H. F. Lau, and M. Hutter, "Vitruvio: An Open-Source Leg Design Optimization Toolbox for Walking Robots," *IEEE Robot. Automat. Lett. (RA-L)*, vol. 5, 2020.
- [6] G. Fadini, T. Flayols, A. del Prete, N. Mansard, and P. Souères, "Computational design of energy-efficient legged robots: Optimizing for size and actuators," in *ICRA2021*, 2020.
- [7] K. Mombaur, "Using optimization to create self-stable human-like running," *Robotica*, vol. 27, 2009.
- [8] G. Buondonno, J. Carpentier, G. Saurel, N. Mansard, A. De Luca, and J.-P. Laumond, "Actuator design of compliant walkers via optimal control," in *IEEE/RSJ IROS*, 2017.
- [9] A. Spielberg, B. Araki, C. Sung, R. Tedrake, and D. Rus, "Functional co-optimization of articulated robots," in *IEEE ICRA*, 2017.
- [10] S. Ha, S. Coros, A. Alspach, J. Kim, and K. Yamane, "Computational co-optimization of design parameters and motion trajectories for robotic systems," *The International Journal of Robotics Research*, vol. 37, 2018.
- [11] R. Desai, B. Li, Y. Yuan, and S. Coros, "Interactive Co-Design of Form and Function for Legged Robots using the Adjoint Method," *arXiv:1801.00385 [cs]*, Apr. 2018, arXiv: 1801.00385. [Online]. Available: <http://arxiv.org/abs/1801.00385>
- [12] M. Geilinger, R. Poranne, R. Desai, B. Thomaszewski, and S. Coros, "Skaterbots: optimization-based design and motion synthesis for robotic creatures with legs and wheels," *ACM Transactions on Graphics*, vol. 37, 2018.
- [13] M. Geilinger, S. Winberg, and S. Coros, "A Computational Framework for Designing Skilled Legged-Wheeled Robots," *IEEE Robot. Automat. Lett. (RA-L)*, vol. 5, 2020.
- [14] B. Amos, I. Jimenez, J. Sacks, B. Boots, and J. Z. Kolter, "Differentiable MPC for End-to-end Planning and Control," in *Advances in Neural Information Processing Systems*, 2018.
- [15] D. P. Kingma and J. Ba, "Adam: A Method for Stochastic Optimization," in *ICLR (Poster)*, 2015.
- [16] R. Featherstone, *Rigid Body Dynamics Algorithms*. Berlin, Heidelberg: Springer-Verlag, 2007.
- [17] R. Budhiraja, J. Carpentier, C. Mastalli, and N. Mansard, "Differential Dynamic Programming for Multi-Phase Rigid Contact Dynamics," in *IEEE-RAS Humanoids*, 2018.
- [18] C. Mastalli, R. Budhiraja, W. Merkt, G. Saurel, B. Hammoud, M. Naveau, J. Carpentier, L. Righetti, S. Vijayakumar, and N. Mansard, "Crocodyl: An Efficient and Versatile Framework for Multi-Contact Optimal Control," in *IEEE ICRA*, 2020.
- [19] C. Mastalli, W. Merkt, J. Marti-Saumell, H. Ferrolho, J. Sola, N. Mansard, and S. Vijayakumar, "A Direct-Indirect Hybridization Approach to Control-Limited DDP," 2021.
- [20] L. Pecyna, A. Cangelosi, and A. Di Nuovo, "A Deep Neural Network for Finger Counting and Numerosity Estimation," in *IEEE Symposium Series on Computational Intelligence (SSCI)*, 2019.
- [21] F. Grimmering, A. Meduri, M. Khadiv, J. Viereck, M. Wüthrich, M. Naveau, V. Berenz, S. Heim, F. Widmaier, T. Flayols, J. Fiene, A. Badri-Spröwitz, and L. Righetti, "An Open Torque-Controlled Modular Robot Architecture for Legged Locomotion Research," *IEEE Robot. Automat. Lett. (RA-L)*, vol. 5, 2020.
- [22] S. Fahmi, C. Mastalli, M. Focchi, and C. Semini, "Passive Whole-Body Control for Quadruped Robots: Experimental Validation Over Challenging Terrain," *IEEE Robot. Automat. Lett. (RA-L)*, vol. 4, 2019.
- [23] G. Bledt, M. J. Powell, B. Katz, J. Di Carlo, P. M. Wensing, and S. Kim, "MIT Cheetah 3: Design and Control of a Robust, Dynamic Quadruped Robot," in *IEEE/RSJ IROS*, 2018.

- [24] N. Hansen, "CMA-ES: A Function Value Free Second Order Optimization Method," in *PGMO COPI*, 2014.
- [25] N. Hansen, Y. Akimoto, and P. Baudis, "CMA-ES/pycma on Github," Zenodo, DOI:10.5281/zenodo.2559634, 2019.

APPENDIX

Previous work has explored the gradient relationship between motion and design on a constrained manifold. These methods do not employ or differentiate a motion planner function. The original idea was introduced by Desai et. al. [11] and popularized by Skaterbots [12] and later [13]. This section describes the technical differences to our work in detail.

A. Skaterbots co-design approach

The authors in [12] begin by describing the motion planning problem as an unconstrained minimization problem. They minimize the so-called energy function, which is a cost function that encodes the centroidal dynamics model and additionally all geometric and velocity constraints of the motion plan. Thus, the motion is computed as:

$$\mathbf{m} = \arg \min_{\hat{\mathbf{m}}} E(\boldsymbol{\rho}, \mathbf{m}), \quad (4)$$

where $E(\cdot)$ is the motion cost. Then, assuming the motion is optimal, the derivative of the motion cost is zero as defined by the first order optimality condition:

$$\frac{\partial E}{\partial \mathbf{m}} = \mathbf{0}. \quad (5)$$

Note that, for clear comparison, we use an explicit notation here to derive the update rule. Then, taking the derivative w.r.t $\boldsymbol{\rho}$ on both sides of (5), they obtain:

$$\frac{\partial}{\partial \boldsymbol{\rho}} \left(\frac{\partial E}{\partial \mathbf{m}} \right) = \frac{\partial^2 E}{\partial \mathbf{m}^2} \frac{\partial \mathbf{m}}{\partial \boldsymbol{\rho}} + \frac{\partial^2 E}{\partial \mathbf{m} \partial \boldsymbol{\rho}} = \mathbf{0}, \quad (6)$$

where one can compute $\frac{\partial \mathbf{m}}{\partial \boldsymbol{\rho}}$ by re-arranging terms and taking the inverse:

$$\frac{\partial \mathbf{m}}{\partial \boldsymbol{\rho}} = - \left(\frac{\partial^2 E}{\partial \mathbf{m}^2} \right)^{-1} \left(\frac{\partial^2 E}{\partial \mathbf{m} \partial \boldsymbol{\rho}} \right). \quad (7)$$

It is important to note that in [12] the co-design metric is defined as a function of \mathbf{m} . However, we can trivially include the design dependency $\boldsymbol{\rho}$. Then, taking the derivative $\nabla_{\boldsymbol{\rho}} J_{cd}(\cdot)$:

$$\nabla_{\boldsymbol{\rho}} J_{cd} = \frac{dJ_{cd}(\boldsymbol{\rho}, \mathbf{m})}{d\boldsymbol{\rho}} = \frac{\partial J_{cd}}{\partial \mathbf{m}} \frac{\partial \mathbf{m}}{\partial \boldsymbol{\rho}} + \frac{\partial J_{cd}}{\partial \boldsymbol{\rho}},$$

we can then substitute $\frac{\partial \mathbf{m}}{\partial \boldsymbol{\rho}}$ from Eq. (6) to obtain the update rule from [12] as:

$$\nabla_{\boldsymbol{\rho}} J_{cd} = - \frac{\partial J_{cd}}{\partial \mathbf{m}} \left(\frac{\partial^2 E}{\partial \mathbf{m}^2} \right)^{-1} \left(\frac{\partial^2 E}{\partial \mathbf{m} \partial \boldsymbol{\rho}} \right) + \frac{\partial J_{cd}}{\partial \boldsymbol{\rho}}. \quad (8)$$

Note that the above update rule is only valid for unconstrained motion planning as derived.